

Lamina-Specific Functional MRI of Retinal and Choroidal Responses to Visual Stimuli

Yen-Yu I. Shib,¹ Bryan H. De La Garza,¹ Eric R. Muir,¹ William E. Rogers,¹ Joseph M. Harrison,² Jeffrey W. Kiel,² and Timothy Q. Duong^{1,2,3,4,5}

PURPOSE. To demonstrate lamina-specific functional magnetic resonance imaging (MRI) of retinal and choroidal responses to visual stimulation of graded luminance, wavelength, and frequency.

MATERIALS AND METHODS. High-resolution ($60 \times 60 \mu\text{m}$) MRI was achieved using the blood-pool contrast agent, monocrystalline iron oxide nanoparticles (MION) and a high-magnetic-field (11.7 T) scanner to image functional changes in the normal rat retina associated with various visual stimulations. MION functional MRI measured stimulus-evoked blood-volume (BV) changes. Graded luminance, wavelength, and frequency were investigated. Stimulus-evoked fMRI signal changes from the retinal and choroidal vascular layers were analyzed.

RESULTS. MRI revealed two distinct laminar signals that corresponded to the retinal and choroidal vascular layers bounding the retina and were separated by the avascular layer in between. The baseline outer layer BV index was 2–4 times greater than the inner layer BV, consistent with higher choroidal vascular density. During visual stimulation, BV responses to flickering light of different luminance, frequency, and wavelength in the inner layer were greater than those in the outer layer. The inner layer responses were dependent on luminance, frequency, and wavelength, whereas the outer layer responses were not, suggesting differential neurovascular coupling between the two vasculatures.

CONCLUSIONS. This is the first report of simultaneous resolution of layer-specific functional responses of the retinal and choroid vascular layers to visual stimulation in the retina. This imaging approach could have applications in early detection and longitudinal monitoring of retinal diseases where retinal and choroidal hemodynamics may be differentially perturbed at various stages of the diseases. (*Invest Ophthalmol Vis Sci.* 2011;52:5303–5310) DOI:10.1167/iovos.10-6438

The retina is nourished by two distinct circulations. The retinal circulation is on the inner retinal surface and projects into the ganglion cell layer, inner plexiform layer, and inner nuclear layer. The choroidal circulation, sandwiched between the retinal pigment epithelium and sclera, supplies the avascular outer nuclear and photoreceptor layers.¹ While both circulations are required for proper retinal function, there are substantial differences between them. For example, choroidal blood flow (BF) is many times greater than retinal BF.^{2,3} There are also significant differences with respect to BF regulation.^{4–8} The choroidal circulation is innervated, while the retinal circulation is not. However, both circulations exhibit pressure-flow autoregulation. The underlying mechanisms of autoregulation appear to differ because the choroid is more responsive to myogenic stimuli⁹ while the retinal circulation is more responsive to retinal metabolism.¹⁰ Imaging methods that can unambiguously resolve evoked responses in the retinal and choroidal vascular layers in vivo would improve understanding of retinal physiology and neurovascular coupling in the retina,^{11,12} which may be important for early detection and longitudinal monitoring of retinal diseases (such as glaucoma¹³ and diabetic retinopathy¹⁴) and testing novel therapeutic strategies for their treatment.

Laser Doppler velocimetry¹⁵ and flowmetry,⁴ laser speckle imaging,^{16,17} and intrinsic optical imaging^{18,19} have been used to image hemodynamic (BF and oxygenation) changes associated with visual and physiological challenges. These optical techniques are generally depth ambiguous, and diseases with media opacity, such as cataract and retinal hemorrhage into the vitreous, may limit the use of optical techniques to study the retina. More recently functional optical coherence tomography of visual stimulation has been reported and, with longer (1060 nm) wavelength, it is possible to detect depth-resolved functional signals (including those from the choroid) and to overcome some media opacity such as cataract (see Ref. 20 for review).

Retinal neurovascular coupling has been studied primarily using flickering light stimulation, which elicits robust increases in retinal and optic nerve head BF, but thus far, most studies have failed to detect changes in choroidal BF in response to flicker stimulation.^{21,22} One potential concern regarding the choroidal flicker response using optical techniques is that BF measurements in humans have been restricted to the subfoveal region. Consequently, a more global choroidal BF or blood volume (BV) measurement with unambiguous retinal and choroidal resolution may provide additional important information.

Magnetic resonance imaging (MRI) has the potential to overcome some of the shortcomings of current in vivo ocular BF measuring techniques as well as to provide complementary information. Compared with optically based imaging techniques, MRI in general has poorer spatiotemporal resolution and signal-to-noise ratio. Work in the brain^{23–25} and the retina^{26–28} suggests that improved MRI spatial resolution could

From the ¹Research Imaging Institute, Departments of ²Ophthalmology, ³Radiology, and ⁴Physiology, University of Texas Health Science Center, San Antonio, Texas; and ⁵South Texas Veterans Health Care System, San Antonio, Texas.

Supported in part by the NIH/NEI (R01 EY014211, EY018855, and R01EY09702), MERIT Award from the Department of Veterans Affairs, and a grant from the San Antonio Life Science Institute to TQD. Y.-Y.I.S. is supported by American Heart Association (10POST4290091) and San Antonio Area Foundation.

Submitted for publication August 19, 2010; revised December 14, 2010, and January 20, 2011; accepted February 9, 2011.

Disclosure: Y.-Y.I. Shib, None; B.H. De La Garza, None; E.R. Muir, None; W.E. Rogers, None; J.M. Harrison, None; J.W. Kiel, None; T.Q. Duong, None

Corresponding author: Timothy Q. Duong, Research Imaging Institute, University of Texas Health Science Center at San Antonio, 8403 Floyd Curl Dr., San Antonio, TX 78229; duongt@uthscsa.edu.

provide global ocular BF, BV, or functional measurements in the retina and choroid with sufficient temporal resolution to detect real-time responses to visual stimulation. Ocular BV responses to flicker stimulation have not yet been studied in rats, although this species is commonly used for models of retinal disease such as diabetic retinopathy, glaucoma, and retinitis pigmentosa.

The goal of the present study was to develop a high-resolution MRI approach to investigate retinal- and choroidal-specific BV responses to visual stimulation in the rat. A high-field (11.7 T) MRI scanner and an established blood-pool MRI contrast agent, monocrystalline iron oxide nanoparticles (MION), were used to improve functional MRI (fMRI) sensitivity.^{29,30} Vascular signals are highlighted because the blood-retinal barrier and retinal pigment epithelium are impermeable to MION. MION has a dephasing effect on the surrounding ¹H₂O MRI signals, so a BV increase in the presence of MION will decrease the fMRI signal. This approach yielded a nominal resolution of 60 × 60 μm and detected layer-specific changes in the retinal and choroidal circulations in response to visual stimulation.

MATERIALS AND METHODS

Animal Preparation

Male Sprague-Dawley rats ($n = 21$, 250–300 g) were initially anesthetized with 2% isoflurane, intubated, and mechanically ventilated (Harvard Ventilator Model 683). The right femoral vein and the lateral tail vein were catheterized. Atropine and phenylephrine eye drops were applied topically to dilate the pupil. After the animal was secured in an MRI-compatible rat stereotaxic headset, isoflurane was discontinued and α -chloralose (60 mg/kg first dose, followed by 30 mg/kg/hr, IV infusion) was administered for anesthesia,^{31–33} followed by pancuronium bromide (4 mg/kg first dose, followed by 4 mg/kg/hr, IV) to eliminate eye movement.^{26,34,35} End-tidal CO₂, rectal temperature, oximetry, and heart rate were continuously monitored and maintained within normal physiological ranges. Mean arterial blood pressure was continuously recorded via a BIOPAC system (Acknowledge, Santa Barbara, CA) in some animals ($n = 3$) via the catheterized femoral artery.

For basal BV studies, an intravascular MION contrast agent (blood half-life >3 hours) was cumulatively administered intravenously at doses of 0, 10, 20, and 30 mg Fe/kg. For fMRI during flicker stimulation, a single dose of 30 mg/kg was used, followed by a second dose of 15 mg/kg after 3 hours if needed. A previous study showed MION did not significantly leak out of the vessels into the retina over time after injection.²⁷

Visual Stimulation

The visual stimulator used a common anode tricolor LED (RL5-RGB TriColor Diffused LED, Superbrightleds.com). The LEDs were coupled to fiber optic cables (Fiberoptic Components, Sterling, MA) using a 2.5 mm glass bundle 8 m in length. An input trigger allowed the scanner to trigger stimulus presentation. Custom-written C++-based software was designed to control, via a graphical user interface, stimulus presentation timing, frequency, luminance, and wavelength. The intensity was controlled by pulse width modulation where the output was modulated by changing the ratio of power on to off time. The LED duty cycle varied from on continuously for maximal brightness to completely off. Each 0.5 ms time unit was divided into on and off times with the minimum on or off time 1/1000th of the time unit.

Visual stimuli were delivered to the animal's eye in the scanner via an MR-compatible optical fiber (2.5 mm in diameter), placed in a preset holder 6 mm away from the eye. The entire retina was illuminated. Each fMRI experiment consisted of five periods of 96 seconds OFF and 96 seconds ON stimulation. Four sets of experiments in which visual stimulation parameters were modulated were studied: (1) 10 Hz flickering achromatic light at a luminance level of 374 cd/m² with a 50%

duty cycle at different MION doses ($n = 9$); (2) stimulus luminance of 81, 234, and 374 cd/m² achromatic flicker at 10 Hz ($n = 9$); (3) stimulus flicker frequency of 1, 10, 30, and 60 Hz achromatic light at a luminance of 374 cd/m² ($n = 7$); (4) stimulus wavelength of red (630 nm), green (525 nm), or blue (472 nm) with 10 Hz flicker and equal quanta of 2.39×10^{15} quanta/s/cm² ($n = 7$). The order of various stimuli was randomized.

MRI Acquisition

MRI studies were performed on an 11.7 T/16 cm magnet and a 74 G/cm gradient insert (B-GA9S; Bruker, Billerica, MA). A custom-made small circular surface coil (ID ~ 7 mm) was placed on the left eye. Magnetic field homogeneity was optimized using FASTMAP shimming with first-order shims on an isotropic voxel of 7 × 7 × 7 mm, encompassing the entire eye. Scout images were acquired to plan a single midsagittal slice bisecting the center of the eye and optic nerve for subsequent imaging to minimize partial-volume effect (PVE) due to the retinal curvature.^{26,34} Basal BV MRIs were measured using a conventional gradient-echo sequence with spectral width = 28 kHz, $TR = 150$ ms, $TE = 5$ ms, $FOV = 7.7 \times 7.7$ mm, slice thickness = 1 mm, acquisition matrix = 256 × 128 (zero-filled to 256 × 256), yielding a nominal resolution of 30 × 30 × 1000 μm. BV fMRI parameters were essentially identical, except spectral width = 14 kHz, acquisition matrix = 128 × 64 (zero-filled to 128 × 128), yielding a nominal in-plane resolution = 60 × 60 × 1000 μm, and temporal resolution = 9.6 seconds.

Data Analysis

Image analysis was performed using a custom-written program (MATLAB, MathWorks, Natick, MA; STIMULATE, University of Minnesota; and Statistical Parametric Mapping [SPM]) as described previously.^{26,36} Briefly, time-series MRI data were coregistered if needed. Changes in the transverse relaxation rate (ΔR_2^*) value vary linearly with BV fraction and were taken as the BV index.³⁰ Basal BV index was calculated pixel by pixel as $\Delta R_2^* = -\ln(S/S_0)/TE$, where S/S_0 is the signal relative to the value before MION injection and TE is the echo time.³⁰ Stimulus-evoked magnitude ΔR_2^* changes were calculated from MRI signals during baseline and stimulation. Percent ΔR_2^* changes were also calculated. Cross-correlation coefficient analysis was performed to obtain activation maps.

For quantitative analysis, the retina was linearized by radially projecting lines perpendicular to the retina. ΔR_2^* profiles were then averaged along the length of the retina.²⁶ FWHM, peak height, and peak separation were determined. Stimulus-evoked percent changes of the raw fMRI signal, stimulus-evoked magnitude changes in ΔR_2^* , and percent ΔR_2^* changes were tabulated for the inner and outer peaks. Statistical analyses of group data were performed by paired *t*-tests and ANOVA. For multiple comparisons, homogeneity of the variances was assessed by Levene's test, and the analyses were followed by a Bonferroni post hoc test. The significance level was set at $P < 0.05$. Results are present as mean ± SD of the mean.

Reproducibility tests included evaluations of activation pattern on repeated trials in the same animals, correlation between odd and even epochs, and intersubject variations by correlation of variation (defined as the SD normalized to the mean of the evoked response across all subjects).³⁷ We did not demonstrate reproducibility on repeated measures on different days on the same animals because these studies were terminal (α -chloralose anesthetic).

RESULTS

Mean arterial blood pressure was measured in three animals. There were no significant differences in mean arterial blood pressure before (123 ± 11 mm Hg) and during (124 ± 11 mm Hg) visual stimulation ($P > 0.05$, paired *t*-test) over the course of the MRI studies.

Basal Retinal and Choroidal Circulations

Figure 1 shows a T_2^* -weighted ($T_2^* \equiv 1/R_2^*$) image of a rat eye before and after three cumulative doses of intravenous MION injections and the corresponding ΔR_2^* images calculated from before and after MION injection. T_2^* -weighted MRI signals on either side of the retina were attenuated after MION injection. The basal ΔR_2^* showed signal changes in two distinct layers, corresponding to the retinal and choroidal circulations. The avascular layer in between only changed slightly, likely because of PVE.^{26,36} The lens and vitreous showed no significant ΔR_2^* MRI signals.

The ΔR_2^* profile analysis across the retinal thickness indicated retinal and choroidal layer thicknesses (full width at half maximum) of 133 ± 18 and $105 \pm 23 \mu\text{m}$ (mean \pm SD, $n = 12$, for the 30 mg/kg MION dose), respectively. The peak-to-peak separation was $166 \pm 21 \mu\text{m}$. The ratios of choroidal to retinal ΔR_2^* peak at 10, 20, and 30 mg/kg MION were 3.93 ± 3.02 , 2.76 ± 2.22 , and 2.02 ± 1.17 , respectively.

Flicker Response as a Function of MION Dosage

fMRI during 10 Hz achromatic flicker was evaluated at different MION doses for optimization (Fig. 2). In the absence of MION, fMRI signals from the whole retina increased during stimulation. With increasing MION doses, stimulus-evoked fMRI signals decreased during stimulation as MION's dephasing effect increasingly dominated. The sensitivity at the dose of 30 mg/kg MION doubled that of no MION at 11.7 T. This dosage is consistent with that used at 11.7 T³⁸ and higher than those used at lower magnetic field for brain fMRI.³⁰ All subsequent experiments used 30 mg/kg MION dose.

Retinal and Choroidal Responses to Flickering Light Stimulation

Figure 3 shows the layer-specific MION fMRI responses. Overlaid scans of the linearized retina showed activation in the inner and outer layers (Fig. 3B). Activation maps are shown for two additional repeated trials in the same rat to

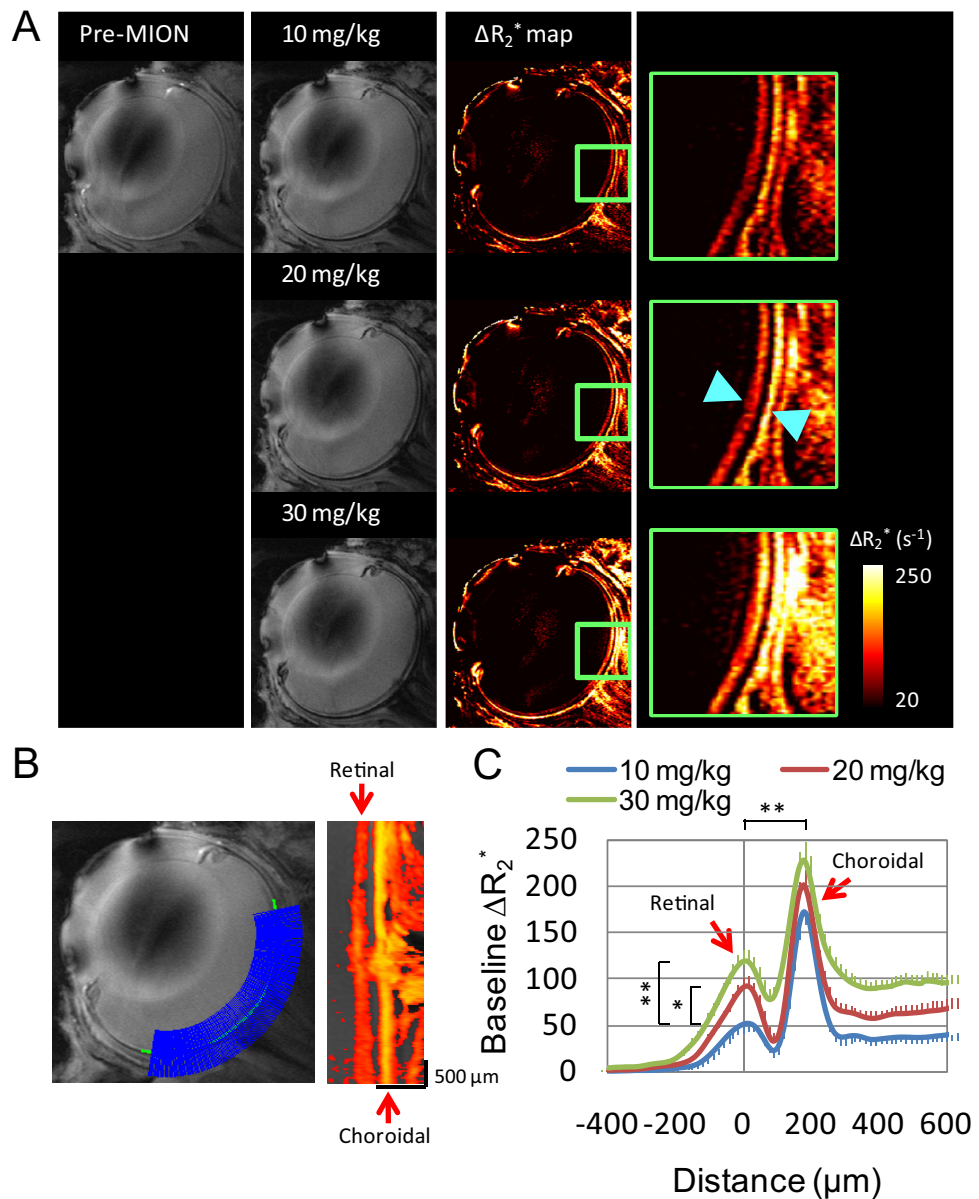


FIGURE 1. Layer-specific basal blood-volume weighted MRI at different doses of MION. **(A)** Gradient-echo MRI was acquired before and after cumulative dose of 10, 20, and 30 mg Fe/kg MION in the same animal. ΔR_2^* maps were calculated and taken as BV index maps. Two blue arrowheads indicate the retinal (inner) and the choroidal (outer) circulation. **(B)** The profiles (blue lines) were radially projected for linearizing the retina ($n = 1$). Basal ΔR_2^* map was color coded and overlaid on the gradient-echo image. The retinal and choroidal vascular layers were distinctly resolved. **(C)** ΔR_2^* profiles (mean \pm SE, $n = 12$) at different MION doses were obtained across the retinal thickness. * $P < 0.05$, ** $P < 0.01$.

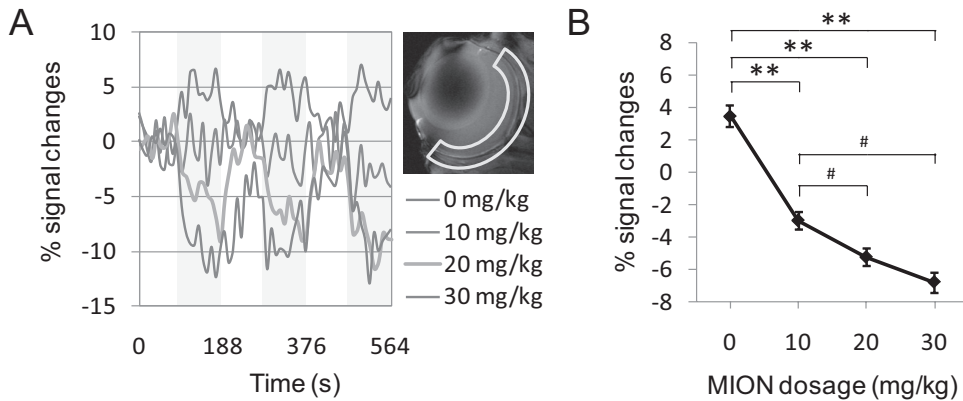


FIGURE 2. fMRI of flicker stimuli at different MION doses. (A) fMRI time courses at different MION doses from a single subject responding to 10 Hz flickering achromatic light. The gray-shaded regions indicate ON stimuli. Time courses were obtained from activated voxels from a ROI (inset). (B) Group-averaged fMRI responses at different MION doses (mean \pm SE, $n = 5$). ** $P < 0.01$, statistical difference from 0 mg/kg MION. # $P < 0.01$, statistical difference from 10 mg/kg MION.

illustrate reproducibility. The activated pixels on the retinal and choroidal vascular layers were highly overlapping between trials. In addition, analysis of reproducibility of odd and even epochs were highly correlated ($r = 0.8797$, $P = 8.37 \times 10^{-19}$). Note that the spread of percentage changes was the results of including all different flicker luminance, color, and frequency as expected. Figure 4 shows the layer-specific MION fMRI responses to 10 Hz flickering light stimulation. The stimulus-evoked ΔR_2^* percent changes were 5% in the inner layer and 1.5% in the outer layer ($P < 0.01$ from baseline without stimulation for both). In absolute units, the magnitude of the ΔR_2^* stimulus-evoked response was also greater in the inner layer ($P < 0.05$). Reproducibility of the 10 Hz flickering light stimulation across the subject pool was further assessed by correlation of variation. The correlations of variation of the ΔR_2^* at the inner and outer

vascular layers were 56% and 63%, respectively (see Discussion).

Regional fMRI Flicker Responses

Laminar-specific fMRI responses to 10 Hz flicker at the optic nerve head region versus more distal regions were compared (Fig. 5). The inner layer response was stronger ($P < 0.01$) at the optic disc region than in the adjacent regions. The stimulus-evoked ΔR_2^* percent changes for all three regions were significantly greater ($P < 0.05$) in the inner than the outer layer. However, the ΔR_2^* magnitude in the optic disc region was larger in the inner than in the outer layer ($P < 0.05$) but not in the adjacent regions. This is likely because of the larger retinal vascular density in the optic nerve head where the central retinal artery enters and central retinal vein exits.

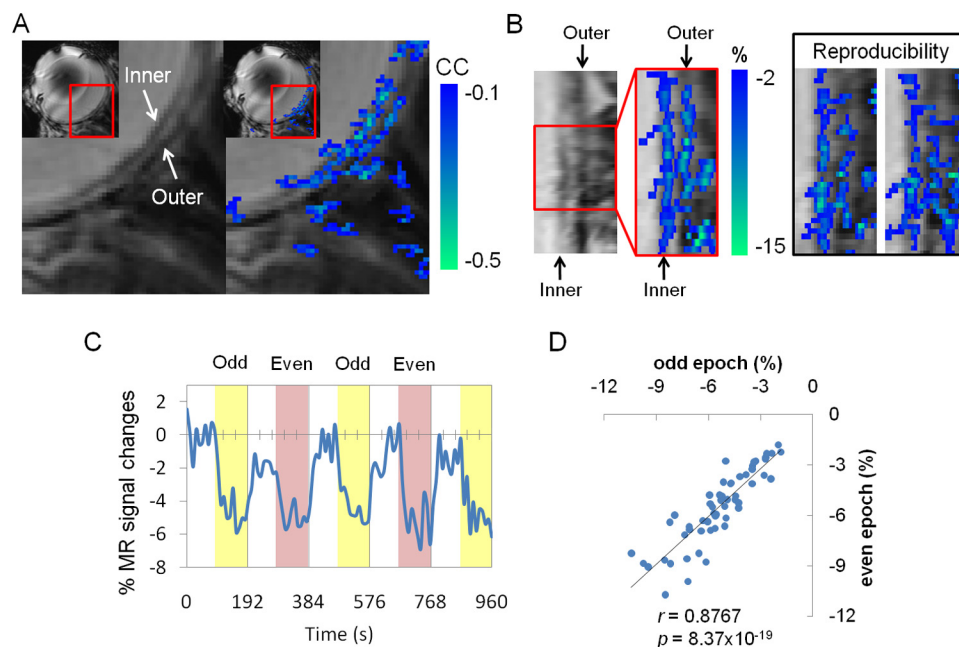


FIGURE 3. Layer-specific MION fMRI response. (A) Cross-correlation maps overlaid on gradient-echo MRI (MION 30 mg/kg). Two arrows in the expanded view indicate the inner and outer bands corresponding to the two vascular layers bounding the retina. (B) Linearized images showed two well-resolved bands activated by visual stimulation. Activation maps are shown for two additional repeated trials in the same rat to illustrate reproducibility within subject. (C) Time course from the activated pixels in (A). The color-shaded regions indicate the stimulus epochs. (D) Reproducibility of the stimulus-evoked response. Percent MR signal changes under different flicker luminance, color, and frequency were included to show the correlation of the even and odd MION fMRI measurements ($n = 8$, total 56 trials). High reproducibility was found between even and odd epochs. Note that the spread of percentage changes was the results of including all different flicker luminance, color, and frequency.

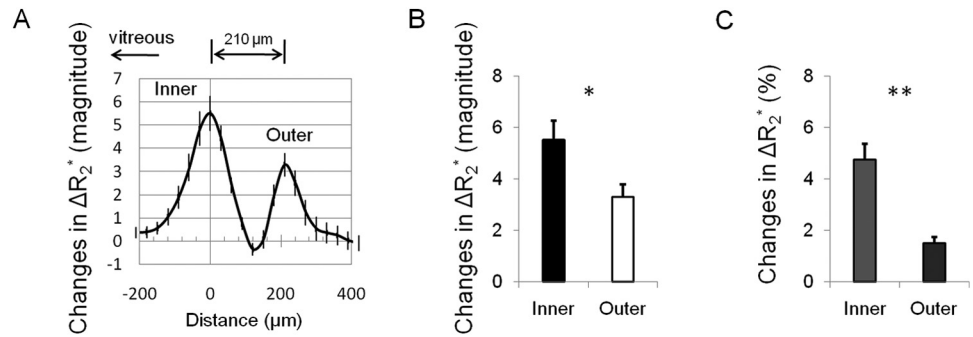


FIGURE 4. Layer-specific MION fMRI of achromatic 10 Hz flicker stimulation. (A) Group-averaged profiles of the stimulus-evoked ΔR_2^* changes across the retinal thickness. The analyzed area was similar as shown in Figure 3B. (B) Magnitude ΔR_2^* and (C) percent ΔR_2^* changes of the inner and outer peaks (mean \pm SE, $n = 18$). * $P < 0.05$, ** $P < 0.01$.

Graded Stimuli

Figure 6A shows the ΔR_2^* responses to three achromatic luminance levels at a fixed flicker frequency of 10 Hz. The inner layer responses increased with increasing luminance from 81 to 234 to 374 cd/m^2 ($n = 9$ each), whereas the outer layer showed no statistically significant trend with respect to changing luminance. Figure 6B shows the ΔR_2^* responses to 1, 10, 30, and 60 Hz flicker frequencies at a fixed achromatic luminance of 374 cd/m^2 ($n = 7$ each). The inner layer responses peaked at 10 Hz. The outer layer showed no statistically significant trend with respect to changing flicker frequency. Figure 6C shows the ΔR_2^* responses to red (630 nm), green (525 nm), and blue (472 nm) light at a fixed 10 Hz flicker frequency with equal light quanta exposure (2.39×10^{13} quanta/s/cm², $n = 7$ each). The inner layer responses to green and blue light were larger than to red light ($P < 0.05$). The outer layer showed no statistically significant trend with respect to changing wavelength.

DISCUSSION

This study demonstrates a novel high-resolution fMRI approach to resolve layer-specific responses to visual stimulation in the rat retina. The major findings are: First, in vivo MRI reveals two distinct laminar signals that correspond to the retinal and choroidal vascular layers bounding the retina, separated by the

avascular layer in between. Basal choroidal ΔR_2^* (BV index) is approximately 2–4 times higher than basal retinal ΔR_2^* . Second, the BV fMRI responses to different graded visual stimuli were consistently detected in the retinal and choroidal vascular layers. Third, the stimulus-evoked MION fMRI magnitude changes of the choroid were comparable with those of retinal vessels, but the stimulus-evoked percent changes of the choroid were significantly smaller than those of the retinal vessels. Fourth, tuning curve characteristics were observed with changing luminance, flicker frequency, and wavelength in the retinal, but not the choroidal, vascular layer. To our knowledge, this is the first report of layer-specific fMRI of visual stimulation in the retina. This approach has the potential to open up new avenues for ocular circulation research and to complement optically based imaging techniques.

Vascular Layer Thickness

The retinal and choroidal thicknesses defined as FWHM of the MION MRI measurements were 133 and 105 μm , respectively, in reasonable agreement with a previous in vivo study using Gd-DTPA (gadolinium diethylenetriamine penta-acetic acid) with T_1 -weighted MRI that found 101 μm for retinal and 86 μm for choroidal thicknesses in rats.²⁶ The slightly greater thickness measured in the present study may be because of the extravascular dephasing effect of MION causing a slightly wider FWHM. Histology showed retinal and choroidal thick-

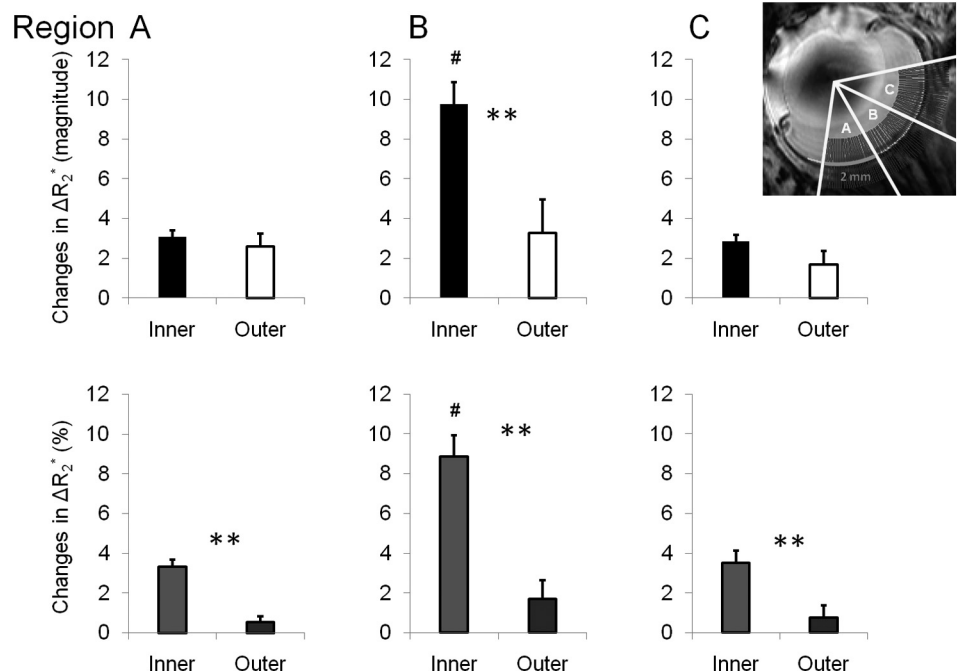


FIGURE 5. Regional differences in magnitude and percent changes of layer-specific MION fMRI (mean \pm SE, $n = 10$). Visual stimulation was achromatic 10 Hz flicker at 374 cd/m^2 . ** $P < 0.01$, statistical difference between inner and outer peak. # $P < 0.01$, statistical difference from regions A and C.

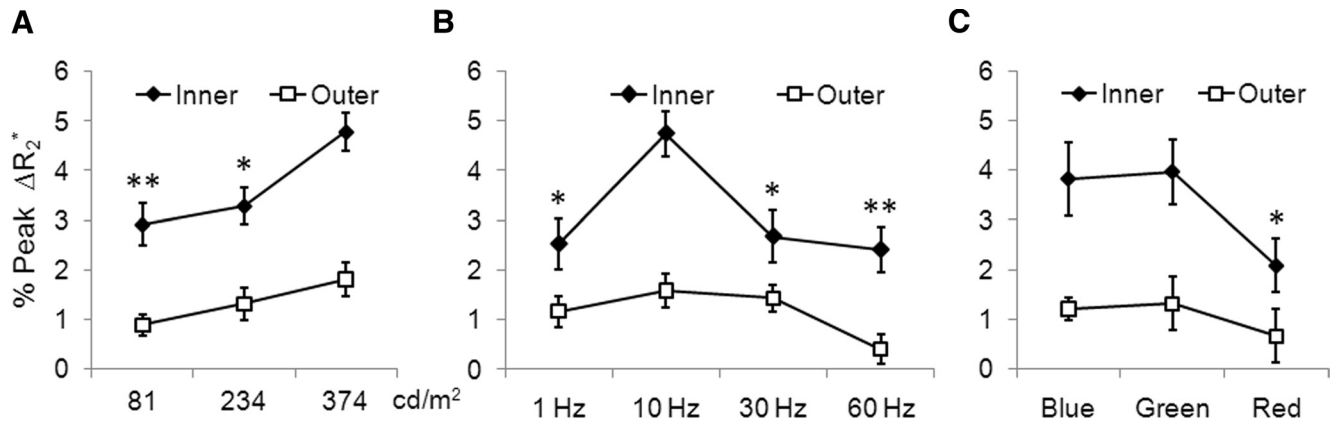


FIGURE 6. (A) Layer-specific MION fMRI of graded luminance ($n = 9$). Layer-specific MION fMRI responses to three different luminances: 81, 234, and 374 cd/m^2 with 10 Hz achromatic light. fMRI responses increased with increasing luminance. * $P < 0.05$, ** $P < 0.01$ indicates statistical difference from 374 cd/m^2 for the inner peak. (B) Layer-specific MION fMRI of graded flicker frequency (mean \pm SE, $n = 7$). Layer-specific MION fMRI responses to four different flicker frequencies: 1, 10, 30, and 60 Hz, with 374 cd/m^2 achromatic light. * $P < 0.05$, ** $P < 0.01$ indicates significant difference from 10 Hz. (C) Layer-specific MION fMRI responses to equal quanta (2.39×10^{15} quanta/s/ cm^2) red, green, and blue with 10 Hz flicker (mean \pm SE, $n = 7$). * $P < 0.05$, statistical difference from green and blue.

ness 92 and 37 μm , respectively.²⁶ The discrepancy between the in vivo and histologic choroidal thicknesses data likely arises from collapse of choroidal vessels after removal of the eye from the influence of the systemic circulation and histologic shrinkage, underscoring the importance of in vivo measurements.

Reproducibility

We performed a few measures of reproducibility. First, the activated pixels on the retinal and choroidal vascular layers from multiple repeated trials in the same animals were highly overlapping between trials (Fig. 3B). Second, the odd and even responses were highly correlated ($r = 0.88$; Fig. 3D). Third, the coefficient of variation of the ΔR_2^* at the inner and outer vascular layers were 56% and 63%, respectively. By comparison, a previous BOLD fMRI reproducibility study reported the coefficient of variation of 50% with hypercapnic challenge and 34% with visual stimulation in human primary visual cortices.³⁷

Basal Blood Volume and Blood Flow Relation

In brain MRI studies, the MION ΔR_2^* signal is widely used as an index of cerebral BV, which varies approximately as the cube root of cerebral BF (i.e., $\Delta\text{volume} = 0.8 \times \Delta\text{flow}^{0.38}$).³⁹ Whether this relationship holds for the retinal and choroidal circulations is unknown. If the cerebral BV-to-BF conversion holds for the choroid and retina, the 2:1 ratio of choroidal to retinal MION ΔR_2^* changes would suggest a choroidal BF \approx 11 times higher than retinal BF, which seems credible.^{2,3} Basal choroidal:retinal BF ratio has been reported to be 11:1 in rats using the microsphere technique² and 6:1 in mice using the arterial spin-labeling BF MRI technique.²⁸ This finding is in qualitative agreement with an earlier MRI study in rats using another intravascular contrast agent, Gd-DTPA, in which the subtraction of post- and precontrast images showed the choroidal vascular layer to be significantly more enhanced than the retinal vascular layer, although no quantitative analysis was performed.²⁶

Effect of Anesthesia

Most MRI studies of animal models require anesthesia, although many awake animal fMRI studies have been reported.^{40–43} Anesthesia alters neural function and hemodynamic responses, potentially resulting in a slower time to

peak and smaller amplitude responses.^{23,44} To minimize these confounding factors, the present study used α -chloralose, which is a widely used anesthetic for fMRI studies owing to its minimal perturbation of neuronal activity.⁴⁵ Other studies demonstrated that neurovascular coupling is preserved in brain under different anesthetics,⁴⁶ including α -chloralose,³¹ pentobarbital,⁴⁷ ketamine-xylazine,⁴⁸ isoflurane,^{40,49} and propofol.⁵⁰ Tight neurovascular coupling between electroretinography and retinal BF responses to flicker stimuli were observed in anesthetized animals.¹⁰ Anesthesia may also impact mean arterial pressure and intraocular pressure. Although mean arterial blood pressure was measured only in some animals, we found no significant differences in mean arterial blood pressure before and during visual stimulation over the course of the MRI studies, consistent with previous studies in similar preparations.^{31,51} Although there was no reason to suspect intraocular pressure to vary over the course of MRI measurements, intraocular pressure was not measured in these animals.

Previous fMRI during Visual Stimulation

Blood oxygenation level-dependent (BOLD) fMRI of the retina using drifting light gratings on the retina was first reported in cats.⁵² BOLD fMRI of the retina using flicker has also been recently demonstrated in rats.⁵³ Both studies found increased BOLD signal as expected. However, neither had sufficient spatial resolution or sensitivity to resolve retinal and choroidal vascular responses. In the present study, BOLD fMRI signals (no MION) from the whole retina increased during stimulation, as expected, due to the decrease in deoxyhemoglobin (an endogenous contrast agent that dephases $^1\text{H}_2\text{O}$ MRI signals) concentration caused by stimulus-evoked BF increase delivering more oxygenated blood (i.e., the BOLD effect). The sensitivity of BOLD fMRI was about half that of MION fMRI at the 30 mg/kg dose. BOLD fMRI of 10 Hz flicker was less reliable in delineating retinal and choroidal vascular responses, likely because echo time herein was not optimized for BOLD contrast at 11.7 T. BOLD fMRI was thus not investigated further using graded visual stimuli. Future studies will explore using optimal BOLD parameters to image retinal and choroidal vascular responses associated with graded visual stimuli. With optimized BOLD contrast, it may be possible that BOLD fMRI could better resolve the two layers in a completely non-invasive manner without the use of contrast agent.

In the brain stimulus-evoked BV^{54,55} and BF increases²⁴ have been reported during various stimulations and tasks using multiple techniques (PET, MRI, autoradiography, and optics), suggesting that BV and BF are tightly coupled in the brain.⁵⁶ In the retina visually evoked BF, blood velocity, and BV increases in retinal vessels have been reported (see Ref. 10 for review). In particular, flicker light stimulation has also been reported to increase BV in optic nerve head rather than blood velocity.²² This finding is consistent with our reports of BV changes by different graded visual stimuli.

Differential Retinal and Choroidal fMRI Responses

Studies in humans and several other nonrodent species show that retinal and optic nerve BF increases during retinal visual stimulation.^{21,22,57} Typically the optic nerve response is greater than the retinal response, though both exhibit roughly exponential responses to luminance and bell-shaped responses to frequency and wavelength using laser Doppler flowmetry, oxygen tension measurements, and electroretinography.^{10,58-60} In keeping with the literature, Figure 5 shows that the retinal MION ΔR_2^* response was greatest in the optic disc region, and Figure 6 shows robust retinal MION ΔR_2^* responses to luminance, frequency, and wavelength. Consistent with the literature, our results show the choroid was largely unresponsive to flicker stimulation and the modulation of the flicker parameters.⁵⁷

In conclusion, the use of a blood-pool contrast agent and a high-field-strength scanner provides sufficient resolution and sensitivity to resolve the rat retinal and choroidal circulations and detect visually evoked retinal and choroidal responses. Retinal vessels respond to changing luminance, frequency, and wavelength, whereas choroidal vessels do not. The key disadvantage of BV fMRI is poorer spatiotemporal resolution and signal-to-noise ratio compared to optically based imaging techniques. Other MRI techniques have been used to image anatomy,^{26,61} relative blood oxygenation,²⁶ BF,²⁸ and functional parameters^{52,53} in the retina. Because MRI can give simultaneous, global information about the ocular circulations without depth limitation and can be done repeatedly, this imaging approach could have applications in early detection and longitudinal monitoring of retinal diseases, such as retinal ischemia, glaucoma, diabetic retinopathy, and retinitis pigmentosa, where retinal and choroidal hemodynamics and neurovascular coupling may be perturbed differently in different diseases and at various disease stages.¹¹ This approach may have clinical applications because similar iron oxide contrast agents are approved for clinical use. Anatomic, BF, and functional MRI studies of the human retina have recently been reported, albeit not yet with laminar resolution.⁶²⁻⁶⁴ In addition, the retinal anatomy with multiple well-defined cellular and vascular layers serves an excellent model to advance MRI technologies to push the boundary of MRI and fMRI spatial resolution.

References

- Harris A, Kagemann L, Cioffi GA. Assessment of human ocular hemodynamics. *Surv Ophthalmol*. 1998;42:509-533.
- Wang L, Grant C, Fortune B, Cioffi GA. Retinal and choroidal vasoreactivity to altered PaCO₂ in rat measured with a modified microsphere technique. *Exp Eye Res*. 2008;86:908-913.
- Alm A, Bill A. The oxygen supply to the retina. II. Effects of high intraocular pressure and of increased arterial carbon dioxide tension on uveal and retinal blood flow in cats. *Acta Physiologica Scand*. 1972;84:306-319.
- Riva CE, Cranstoun SD, Mann RM, Barnes GE. Local choroidal blood flow in the cat by laser Doppler flowmetry. *Invest Ophthalmol Vis Sci*. 1994;35:608-618.
- Kergoat H, Faucher C. Effects of oxygen and carbogen breathing on choroidal hemodynamics in humans. *Invest Ophthalmol Vis Sci*. 1999;40:2906-2911.
- Riva CE, FPournaras CJ, Tsacopoulos M. Regulation of local oxygen tension and blood flow in the inner retina during hyperoxia. *J Appl Physiol*. 1986;61:592-598.
- Rassam SMB, Patel V, Chen HC, Kohner EM. Regional retinal blood flow and vascular autoregulation. *Eye*. 1996;10:331-337.
- Riva CE, Cranstoun SD, Grunwald JE, Petrig BL. Choroidal blood flow in the foveal region of the human ocular fundus. *Invest Ophthalmol Vis Sci*. 1994;35:4273-4281.
- Kiel JW, Shepherd AP. Autoregulation of choroidal blood flow in the rabbit. *Invest Ophthalmol Vis Sci*. 1992;33:2399-2410.
- Riva CE, Logean E, Falsini B. Visually evoked hemodynamical response and assessment of neurovascular coupling in the optic nerve and retina. *Progress Retinal Eye Res*. 2005;24:183-215.
- Pournaras CJ, Rungger-Brandle E, Riva CE, Hardarson SH, Stefansson E. Regulation of retinal blood flow in health and disease. *Prog Retin Eye Res*. 2008;27:284-330.
- Riva CE, Falsini B. Functional laser Doppler flowmetry of the optic nerve: physiological aspects and clinical applications. *Prog Brain Res*. 2008;173:149-163.
- Gugleta K, Fuchsjäger-Mayrl G, Orgul S. Is neurovascular coupling of relevance in glaucoma? *Surv Ophthalmol*. 2007;52(Suppl 2):S139-143.
- Pemp B, Schmetterer L. Ocular blood flow in diabetes and age-related macular degeneration. *Can J Ophthalmol*. 2008;43:295-301.
- Riva CE, Grunwald JE, Singclair SH. Laser Doppler velocimetry study of the effect of pure oxygen breathing on retinal blood flow. *Invest Ophthalmol Vis Sci*. 1983;24:47-51.
- Cheng H, Duong TQ. Simplified laser-speckle-imaging analysis method and its application to retinal blood flow imaging. *Opt Lett*. 2007;32:2188-2190.
- Cheng H, Yan Y, Duong TQ. Temporal statistical analysis of laser speckle image and its application to retinal blood-flow imaging. *Opt Express*. 2008;16:10214-10219.
- Grinvald A, Bonhoeffer T, Vanzetta I, et al. High-resolution functional optical imaging: from the neocortex to the eye. *Ophthalmol Clin North Am*. 2004;17:53-67.
- Tsunoda K, Oguchi Y, Hanazona G, Tanifuji M. Mapping cone- and rod-induced retinal responsiveness in macaque retina by optical imaging. *Invest Ophthalmol Vis Sci*. 2004;45:3820-3826.
- Drexler W, Fujimoto JG. State-of-the-art retinal optical coherence tomography. *Prog Retin Eye Res*. 2008;27:45-88.
- Riva CE, Logean E, Falsini B. Temporal dynamics and magnitude of the blood flow response at the optic disk in normal subjects during functional retinal flicker-stimulation. *Neurosci Lett*. 2004;356:75-78.
- Garhofer G, Huemer KH, Zawinka C, Schmetterer L, Dorner GT. Influence of diffuse luminance flicker on choroidal and optic nerve head blood flow. *Curr Eye Res*. 2002;24:109-113.
- Duong TQ, Kim DS, Ugurbil K, Kim SG. Spatiotemporal dynamics of the BOLD fMRI signals: toward mapping submillimeter cortical columns using the early negative response. *Magn Reson Med*. 2000;44:231-242.
- Duong TQ, Kim DS, Ugurbil K, Kim SG. Localized cerebral blood flow response at submillimeter columnar resolution. *Proc Natl Acad Sci USA*. 2001;98:10904-10909.
- Silva AC, Koretsky AP. Laminar specificity of functional MRI onset times during somatosensory stimulation in rat. *Proc Natl Acad Sci USA*. 2002;99:15182-15187.
- Cheng H, Nair G, Walker TA, et al. Structural and functional MRI reveals multiple retinal layers. *Proc Natl Acad Sci USA*. 2006;103:17525-17530.
- Nair G, Tanaka Y, Kim M, et al. MRI reveals differential regulation of retinal and choroidal blood volumes in rat retina. *Neuroimage*. 2011;54:1063-1069.
- Muir ER, Duong TQ. MRI of retinal and choroid blood flow with laminar resolution. *NMR Biomed*. 2011;24:216-223.

29. Shen T, Weissleder R, Papisov M, Bogdanov A, Jr., Brady TJ. Monocrystalline iron oxide nanocompounds (MION): physicochemical properties. *Magn Reson Med.* 1993;29:599-604.
30. Mandeville JB, Marota JJ, Kosofsky BE, et al. Dynamic functional imaging of relative cerebral blood volume during rat forepaw stimulation. *Magn Reson Med.* 1998;39:615-624.
31. Duong TQ, Silva AC, Lee SP, Kim SG. Functional MRI of calcium-dependent synaptic activity: cross correlation with CBF and BOLD measurements. *Magn Reson Med.* 2000;43:383-392.
32. Shih YY, Chen CC, Shyu BC, et al. A new scenario for negative functional magnetic resonance imaging signals: endogenous neurotransmission. *J Neurosci.* 2009;29:3036-3044.
33. Shih YY, Chen YY, Chen CC, Chen JC, Chang C, Jaw FS. Whole-brain functional magnetic resonance imaging mapping of acute nociceptive responses induced by formalin in rats using atlas registration-based event-related analysis. *J Neurosci Res.* 2008;86:1801-1811.
34. Li Y, Cheng H, Duong TQ. Blood-flow magnetic resonance imaging of the retina. *Neuroimage.* 2008;39:1744-1751.
35. Li Y, Cheng H, Shen Q, et al. Blood-flow magnetic resonance imaging of retinal degeneration. *Invest Ophthalmol Vis Sci.* 2009;50:1824-1830.
36. Duong TQ, Muir ER. Magnetic resonance imaging of the retina. *Jpn J Ophthalmol.* 2009;53:352-367.
37. Leontiev O, Buxton RB. Reproducibility of BOLD, perfusion, and CMRO₂ measurements with calibrated-BOLD fMRI. *NeuroImage.* 2007;35:175-184.
38. Keilholz SD, Silva AC, Raman M, Merkle H, Koretsky AP. BOLD and CBV-weighted functional magnetic resonance imaging of the rat somatosensory system. *Magn Reson Med.* 2006;55:316-324.
39. Grubb RL, Raichle ME, Eichling JO, Ter-Pogossian MM. The effects of changes in PaCO₂ on cerebral blood volume, blood flow, and vascular mean transit time. *Stroke.* 1974;5:630-639.
40. Sicard K, Shen Q, Brevard ME, et al. Regional cerebral blood flow and BOLD responses in conscious and anesthetized rats under basal and hypercapnic conditions: implications for functional MRI studies. *J Cereb Blood Flow Metab.* 2003;23:472-481.
41. Logothetis NK, Guggenberger H, Peled S, Pauls J. Functional imaging of the monkey brain. *Nature Neurosci.* 1999;2:555-562.
42. Ferris CF, Snowdon CT, King JA, et al. Activation of neural pathways associated with sexual arousal in non-human primates. *J Magn Reson Imag.* 2004;19:168-175.
43. Martin C, Martindale J, Berwick J, Mayhew J. Investigating neural-hemodynamic coupling and the hemodynamic response function in the awake rat. *Neuroimage.* 2006;32:33-48.
44. Kim SG, Duong TQ. Mapping cortical columnar structures using fMRI. *Physiol Behav.* 2002;77:641-644.
45. Ueki M, Mies G, Hossmann KA. Effect of alpha-chloralose, halothane, pentobarbital and nitrous oxide anesthesia on metabolic coupling in somatosensory cortex of rat. *Acta Anaesthesiol Scand.* 1992;36:318-322.
46. Franceschini MA, Radhakrishnan H, Thakur K, et al. The effect of different anesthetics on neurovascular coupling. *NeuroImage.* 2010;51:1367-1377.
47. Hyder F, Behar K, Martin M, Blamire A, Shulman R. Dynamic magnetic resonance imaging of the rat brain during forepaw stimulation. *J Cereb Blood Flow Metab.* 1994;14:649-655.
48. Shih YY, Chang C, Chen JC, Jaw FS. BOLD fMRI mapping of brain responses to nociceptive stimuli in rats under ketamine anesthesia. *Med Eng Phys.* 2008;30:953-958.
49. Masamoto K, Kim T, Fukuda M, Wang P, Kim SG. Relationship between neural, vascular, and BOLD signals in isoflurane-anesthetized rat somatosensory cortex. *Cereb Cortex.* 2007;17:942-950.
50. Lahti KM, Ferris CF, Li F, Sotak CH, King JA. Comparison of evoked cortical activity in conscious and propofol-anesthetized rats using functional MRI. *Magn Reson Med.* 1999;41:412-416.
51. Sicard KM, Duong TQ. Effects of hypoxia, hyperoxia and hypercapnia on baseline and stimulus-evoked BOLD, CBF and CMRO₂ in spontaneously breathing animals. *NeuroImage.* 2005;25:850-858.
52. Duong TQ, Ngan S-C, Ugurbil K, Kim S-G. Functional magnetic resonance imaging of the retina. *Invest Ophthalmol Vis Sci.* 2002;43:1176-1181.
53. De La Garza B, Li G, Muir E, Shih YY, Duong TQ. Blood oxygenation level-dependent (BOLD) fMRI of visual stimulation in the rat retina at 11.7 T. *NMR Biomed.* 2011;24:188-193.
54. Hillman EM, Devor A, Bouchard MB, et al. Depth-resolved optical imaging and microscopy of vascular compartment dynamics during somatosensory stimulation. *NeuroImage.* 2007;35:89-104.
55. Kim T, Hendrich KS, Masamoto K, Kim SG. Arterial versus total blood volume changes during neural activity-induced cerebral blood flow change: implication for BOLD fMRI. *J Cereb Blood Flow Metab.* 2007;27:1235-1247.
56. Raichle ME. Behind the scenes of functional brain imaging: a historical and physiological perspective. *Proc Natl Acad Sci USA.* 1998;95:765-772.
57. Garhofer G, Zawinka C, Resch H, Huemer KH, Dorner GT, Schmetterer L. Diffuse luminance flicker increases blood flow in major retinal arteries and veins. *Vision Res.* 2004;44:833-838.
58. Shakoor A, Blair NP, Mori M, Shahidi M. Choriorretinal vascular oxygen tension changes in response to light flicker. *Invest Ophthalmol Vis Sci.* 2006;47:4962-4965.
59. Neitz J, Jacobs GH. Reexamination of spectral mechanisms in the rat (*Rattus norvegicus*). *J Comp Psychol.* 1986;100:21-29.
60. Jacobs GH, Neitz J, Deegan JF 2nd. Retinal receptors in rodents maximally sensitive to ultraviolet light. *Nature.* 1991;353:655-656.
61. Shen Q, Cheng H, Pardue MT, et al. Magnetic resonance imaging of tissue and vascular layers in the cat retina. *J Magn Reson Imag.* 2006;23:465-472.
62. Zhang Y, Peng Q, Kiel JW, Rosende CA, Duong TQ. Magnetic resonance imaging of vascular oxygenation changes during hyperoxia and carbogen challenges in the human retina. *Invest Ophthalmol Vis Sci.* 2011;52:286-291.
63. Peng Q, Zhang Y, Oscar San Emeterio Nateras O, van Osch MJP, Duong TQ. Magnetic resonance imaging of blood flow of the human retina. *Magn Reson Med.* 2011;65:1768-1775.
64. Maleki N, Dai W, Alsop DC. Blood flow quantification of the human retina with MRI. *NMR Biomed.* 2011;24:104-111.